ICES Journal of Marine Science, 2024, Vol. 0, Issue 0, 1–9
https://doi.org/10.1093/icesjms/fsae032
Received: 30 June 2023; **revised:** 16 February 2024; **accepted:** 22 February 2024
Review Article

Implementation of the split-beam function to Mills cross multibeam echo sounder for target strength measurements

Guillaume Matte[1,*], Tehei Gauthier[1], Nathan Rousselot[1], Jean Guillard[2], Marie Lamouret[1], Olivier Lerda[1], Benoit Tallon[3], Phillipe Roux[4], Frederic Mosca[1]

[1]Exail SONAR, 13600 La Ciotat, France
[2]Universite Savoie Mont Blanc, INRAE, CARRTEL,74 200 Thonon-les Bains, France
[3]Institut Jean le Rond d'Alembert, Sorbonne University, 75002 Paris, France
[4]ISTerre, CNRS, 38058 Grenoble, France

*Corresponding author. Exail SONAR, 46 quai François Mitterrand, 13600 la Ciotat, France, E-mail: guillaume.matte@exail.com

Abstract

Modern challenges in the increasing exploitation of aquatic ecosystems require efficient, reliable, and noninvasive technologies to acquire biomass information on a large scale. For the past 40 years, hydroacoustics has been an essential tool to analyse fish populations and their relationship with the environment. Currently, split-beam echo sounders are standard tools used to reliably and accurately record data in oceans, estuaries, and lakes. To maximize the coverage volume and to increase target detection, and therefore data quality, the use of multi-beam echo sounders is a real asset. We propose here an innovative method for target strength (TS) calculation based on the signal from a reversible Mills cross multi-beam sonar, SeapiX (Exail), which also includes the analytical capability of a split-beam echo sounder. This innovative approach provides new original information when using a multi-beam sonar. The case study in Lake Bourget was based on a comparison of the simultaneous recordings of SeapiX and EK80 (SIMRAD) to prove the validity of this multi split-beam processing, as well as to estimate the *in situ* TS of fish.

Keywords: multi-beam; target strength; split-beam

Introduction

The global transition to renewable energy sources in response to climate change has spurred the development of large-scale projects involving the installation of massive energy structures that affect both marine and lake ecosystems. This trend necessitates a comprehensive analysis of fish resources and ecosystems to address the challenges posed by the deployment of energy generators using wind, waves, or tidal energy in marine areas and the increasing use of thermal energy, wind turbines, and photovoltaic panels in large lakes and reservoirs (Fink et al. 2014).

For the past decades, echo sounders have played key roles in observing, quantifying, and analysing fish populations (Simmonds and MacLennan 2008). The instruments most commonly used to conduct abundance estimation assessments are still split-beam echo sounders (SBES), which are operated from conventional vessels. The increasing stress on marine ecosystems due to human impacts, such as industrial fishing, the deployment of renewable energy on large scales, and climate change, has increased the demand for more efficient methods for monitoring the status of impacts on ecosystems components and function. To enhance the acoustic sampling volume and expand the observations of fish behaviors, such as avoidance, the use of a multibeam echo sounder (MBES) in routine surveys should be considered. The MBES data provide an additional spatial dimension of fish distribution in the water column, i.e. whether the fish are scattered or aggregated in the shoals. Topological analysis, such as that described by Petitgas and Levenez (1996), can be performed in three dimensions, considering the topological characteristics of schools as potential markers of fish species (Scalabrin et al. 1996, Proud et al. 2020).

MBESs have been employed to conduct water column analyses, and they enable backscattering measurements, single echo detection (SED), and volumetric imaging of fish schools (Colbo et al. 2014). Initial pioneering efforts were directed toward qualitatively visualizing the water column using standard hydrographic MBES (Gerlotto et al. 1999). Innovations in displaying MBES data for fishery research then progressively capitalized on advancing 3D graphical display technology (Mayer et al. 2002), and these innovative 3D visualization tools have significantly transformed the approach used to comprehend water column data. Acoustic calibration methods were subsequently refined for application in MBESs, facilitating the quantitative assessment of water column data (Foote 2006). However, despite this advancement, the technique has not been applied on an industrial scale to date, neither within the scientific community nor among MBES manufacturers.

The main aim of this study was to evaluate the compatibility of SeapiX MBES calibrated data with historical echosounding datasets, ensuring a seamless integration with existing research methodologies. In this respect, we have evaluated the performance of the SeapiX MBES (Exail, la Ciotat France) in assessing target strength (TS), a crucial metric used to

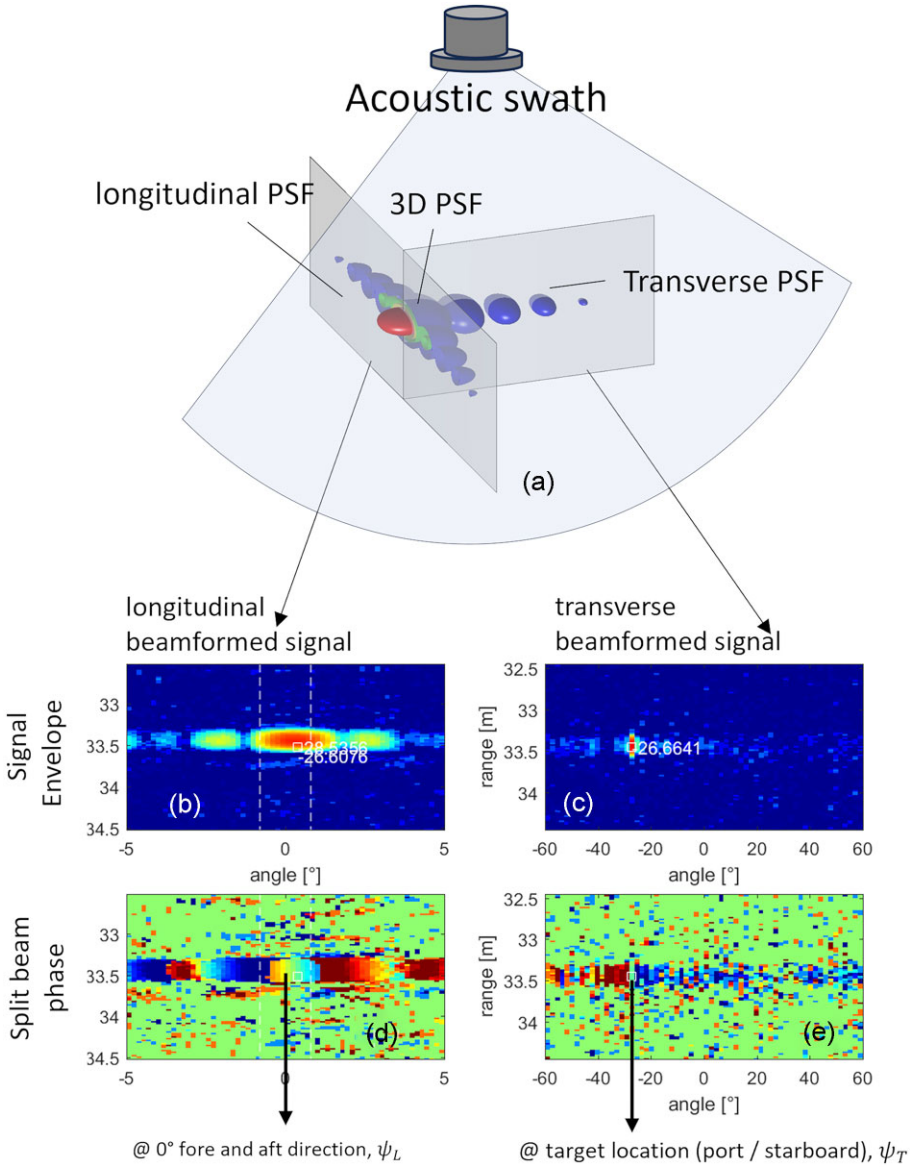

Figure 1. Beamformed signal matrix decomposition. (a) represents the acoustic swath acquired in one ping (which is a transmission and reception sequence). A target is represented as the 3D PSF of the imaging system (SeapiX). This 3D PSF can be decomposed in two dimensions: (b) the longitudinal beamformed signal and (c) the transverse beamformed signal (the envelope of the signal is displayed in dB). (d) and (e) are a representation of the split-beam phase (or interferometric phase).

determine the size and density of fish populations and for monitoring individual behavior. We also compared the efficiency of the SeapiX MBES with that of conventional SBES by conducting a measurement campaign on a well-known fish population (*Coregonus lavaretus*) in Lake Bourget in 2019 (Mouget et al. 2019a, Rautureau et al. 2022). Our study findings contribute to ensuring continuity and comparability of long-term ecological monitoring efforts, thereby facilitating the integration of novel technologies into established research frameworks.

Materials and methods

Hardware description

To avoid a common confusion between the terms "beam" and "transducer," we will refer to the MBES transmit/receive elements as the transducer array throughout this document. The transducer is the active element that converts electrical signal into an ultrasound wave. The beam is the result of coherent interferences between the ultrasound waves generated by the array of transducers, therefore pointing toward a specific direction. SeapiX MBES (Mosca et al. 2016) consists of two uniform linear transducer arrays with 64 elements each, arranged in a Mills cross. SeapiX MBES is symmetric, transmission/reception reversible, and electronically steerable. It provides transverse (i.e. across-track) or longitudinal (along-track) acoustic swaths of 120° by 1.6°, tiltable by 45°, giving the ability to see cross sections of the water column (Fig. 1). The transmission pulsers and digitalization electronics are embedded in the subsea sonar head in the close vicinity of the transducers in order to keep the electronic noise level as low as possible. The connection between the sonar head and the processing computer is simply made by a subsea cable carrying power supply, ethernet for data stream

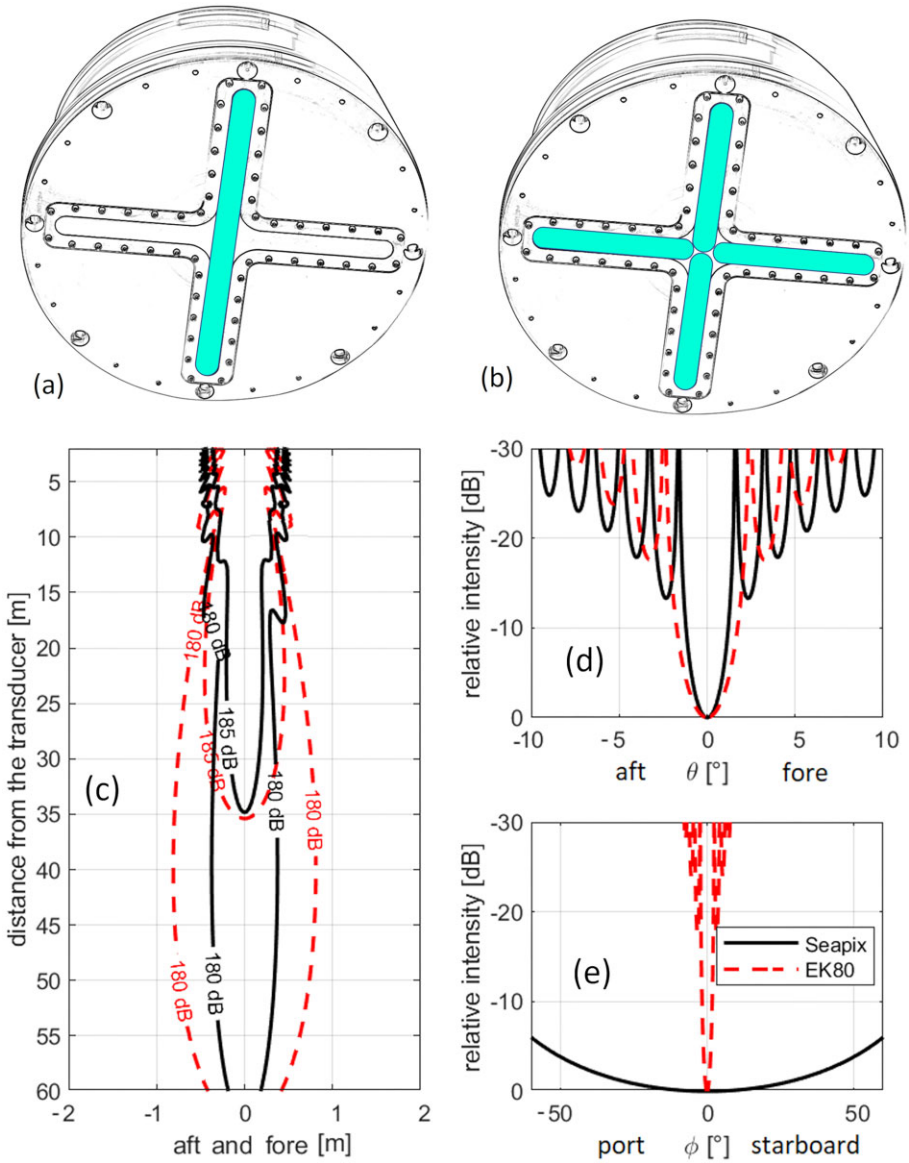

Figure 2. SeapiX transducers and beam patterns. Transmitted beam with the longitudinal transducer array (a), received beams from all parts (b), theoretical spatial distribution of sound level in the water column for SeapiX (solid line) and EK80 (dashed line) (c). Longitudinal (d) and transverse (e) beam profile comparison for SeapiX (solid line) and EK80 (dashed line).

communication, and a coax for signal synchronization. Figure 1 shows the SeapiX transverse swath mainly used in this study. Considering an ideal imaginary point target, the impulse response of the SeapiX imaging system can be called a point spread function (PSF), which is represented in Fig. 1 in three dimensions. The two cross sections of the PSF in Fig. 1a are decomposed as the amplitude shown in Fig. 1b and c and the interferometric phase (or split-beam phase) shown in Fig. 1d and e. Figure 2a and b depicts the transmission/reception sequence illustrating the contribution of each transducer array segment during the transmission (longitudinal transducer array being on Fig. 2a) and the reception of the backscattered signal (all of the transducer array segments being on Fig. 2b). To illustrate the differences in beam dimensions, the transmission beam profiles for the SeapiX MBES and EK80 have been overlaid in Fig. 2, specifically in parts c–e. The sound level of both systems at the surface of each transducer was assumed to be equivalent. The main beam cross section 2c shows the difference between the EK80 120 kHz (dashed red lines) and SeapiX 150 kHz (solid black lines) in the aft and fore directions. In Fig. 2d and e, the transmission beams are displayed angularly. The most explicit view of the angular difference between the SBES and the MBES is the wide acoustic beam displayed in Fig. 2e.

Physical quantities

Once the acoustic pulse is emitted by the longitudinal transducer array—one of the two arrays—the raw acoustic signal is acquired simultaneously by each of all 128 transducers (from both transducer arrays) at a rate of 3 MHz. Subsequently, each of the 128 signals undergoes filtering, compensation for time variable gain (TVG), demodulation, decimation, and downsampling to 43 kHz. SeapiX beamforming employs delay and sum beamforming at a baseband and produces 64–256 beams in real time from both receiving arrays (i.e. 128–512 simultaneous beams). In this study, the number of calculated beams was set to 64 aiming to minimize the size of the files to process

and to create a proof of concept for the inter beam compensation as explained in Equation (9). The beamformed signal matrix $S(n_b,\ t)$ contains the signal variation over time in one dimension (t), and it is a function of the angle in the other dimensions, denoted as the beam number (n_b). This is the principal component for computing physical quantities. In practice, the split-beam phase is determined by the phase difference between the half-transducer arrays. For example, the signals from the first 32 transducers were beamformed in 64 directions. The same operation is performed with the signals from the other 32 transducers of the same transducer array. The resulting signal matrix is called the split-beam signal matrix. After demodulation, the signals from both split-beams are decimated, and each sample is a complex number. The split-beam matrices are combined to extract the swath echogram modulus and phase.

$S(n_b,\ t)$ is converted to the echo-level (EL) using the following sonar Equation (1):

$$\mathrm{EL}\,(n_b,t) = 10\log_{10}\left(S(n_b,t)^2\right) - G\,(t) - \mathrm{RVS} - F, \quad (1)$$

where n_b is the beam number, t is the time of the recorded sample, $G(t)$ is the TVG [dB], RVS is the receive voltage response [dB re 1 V/dBμPa], and F is the chain factor conversion [dB re 1 bits/V]. $S(n_b,\ t)$ is the demodulated and decimated beamformed signal. It is expressed in bits. The signal $S(n_b,\ t)$ has been amplified by a TVG $G(t)$. This amplification occurs in the analog electronics. To recover numerically the signal metrological values, $G(t)$ must be removed from $S(n_b,\ t)$. From the EL, the TS was calculated using Equation (9).

$$\mathrm{TS}\,(n_b,t) = \mathrm{EL}\,(n_b,t) - \mathrm{SL} + 40\log_{10}(r) + 2\alpha r + C\,(n_b) \\ -20\log_{10}(\mathrm{sinc}(\psi_L\,(n_b,t)\,\mathrm{sinc}\,(\psi_T\,(n_b,t))\,, \quad (2)$$

where SL is the transmitted Sound level [dB rel. 1μPa at 1 m], r is the range [in meters], α is the absorption of sound expressed in [dB/m], and C is a vector of correction level values derived from the calibration [in dB]. In practical terms, the transducer array was not treated as an infinitely thin line; an additional correction was introduced to consider the transducer array finite dimensions. Therefore, $C \approx 50\ \log10(\cos\theta_{nb})$ accounts for the two-ways mean directivity of the transducers composing the array. Here, ψ_T and ψ_L denote the split-beam phase signals of the transversal and longitudinal swaths, respectively. These split-beam phases are computed based on a combination of half-transducer array signals achieved through delay-and-sum beamforming of the transducer subarrays (where each subarray comprises half the length of the transducer arrays).

To elaborate further, ψ_T is the phase difference between the beamformed signal by the starboard side of the transducer array and the beamformed signal by the port side of the array. Simultaneously, ψ_L is the difference between the phase of the beamformed signal by the foreside of the transducer array and the aft side of the transducer array. Let $S_{T1}(n_b,\ t)$ be the beamformed signal of the starboard side, and $S_{T2}(n_b,\ t)$ be the beamformed signal of the port side. Because these signals are complex numbers, the real and imaginary parts must be used as

$$\psi_{T1}\,(n_b,t) = \mathrm{atan}(\Im\,[S_{T1}\,(n_b,t)]\,,\ \Re\,[S_{T1}\,(n_b,t)]\,, \quad (3)$$

$$\psi_{T2}\,(n_b,t) = \mathrm{atan}(\Im\,[S_{T2}\,(n_b,t)]\,,\ \Re\,[S_{T2}\,(n_b,t)]\,, \quad (4)$$

where $\Re$ represents the real component of a complex number, and $\Im$ represents the imaginary component. Also, atan returns the arctangent of the input argument ratio over $[-\frac{\pi}{2}\ \frac{\pi}{2}]$. The transverse split-beam phase becomes

$$\psi_T\,(n_b,t) = \psi_{T2}\,(n_b,t) - \psi_{T1}\,(n_b,t) \quad (5)$$

in the same way as S_{L1}being the beamformed signal of the foreside and S_{L2} the beamformed signal of the aft side.

$$\psi_L\,(n_b,t) = \psi_{L2}\,(n_b,t) - \psi_{L1}\,(n_b,t)\,. \quad (6)$$

The ψ_L being the longitudinal split-beam phase.

In the case of fully developed speckle from a fish school or aggregation backscattering, the volume backscattering strength SV is given by Equations (7) and (8).

$$\mathrm{SV}\,(n_b,t) = \mathrm{EL}\,(n_b,t) - \mathrm{SL} + 40\log_{10}(r) + 2\alpha r \\ -10\log_{10}V\,(n_b,t) + C\,(n_b) \quad (7)$$

with

$$V\,(n_b,t) = \theta_{-3dB}\,(n_b)\,\phi_{-3dB}r^2\left(\frac{ct}{2}\right), \quad (8)$$

where $\theta_{-3dB}(n_b)$ is the beamwidth at -3 dB of the nth received beam, ϕ_{-3dB} is the beamwidth at -3 db of the nth transmitted beam. Both are expressed in radians. c is the speed of sound [m/s]. The signal matrices S, EL, TS, and SV are explicitly denoted as $S(n_b,\ t)$, EL$(n_b,\ t)$, TS$(n_b,\ t)$, and SV$(n_b,\ t)$ to express the pixel value of the final image. The indices n_b and t, respectively, stand for "beam number" and "sampling time in seconds." In the literature, SV is often written as depending on 20 log10 r (Simmonds and MacLennan 2008). We deliberately chose here to express it in a very similar manner when compared to the TS expression with a dependency of 40 log10 r because the SV is homogeneous to a TS normalized by the resolution cell $V\ (n_b,\ t)$, which contains the required r^2. However, the SV equation does not need to account for the inter-beam compensation because the energy is integrated over the entire received beam.

Pixel-based TS calculation

TS calculation was not only performed on single targets, but over the whole split-beam matrices. To achieve this, beamformed data was conceptualized as an image—a representation of acoustic intensity mapped with respect to time samples arriving from specific directions. Each time sample corresponds to a range ($r = c.\frac{t}{2}$) and the direction is defined by the beamformed angle. The pixel-based TS calculation yields Equations (1) and (9), where $r = c.\frac{t}{2}$:

$$\mathrm{TS}\,(n_b,t) = 20\log_{10}(S\,(n_b,t)) - G\,(t) - \mathrm{RVS} - F - \mathrm{SL} + \mathrm{PG} \\ + 40\log_{10}\left(\frac{ct}{2}\right) + \frac{2\alpha ct}{2} + C\,(n_b) \\ - 20\log_{10}(\mathrm{sinc}\,(\psi_T\,(n_b,t))\,.\mathrm{sinc}\,(\psi_L\,(n_b,t)) \quad (9)$$

with PG the processing gain brought on by pulse compression in a case where chirp modulated signal would be transmitted. If a tone burst is selected, PG would be 0. The impact of the dispersion brought on by the employment of multiple transducers—each with unique efficiencies, or subject to positional errors—is confined to the secondary lobes. Interestingly, the main lobe retains its original structure and remains unaffected, even with eventual transducer loss. Based on this observation, we can take advantage of the analytical expression provided in the equation to model the behavior of the transmission/reception lobes effectively.

Case study: lake bourget fish TS measurement

To demonstrate the practical feasibility of this calibration in *in situ* operations, we conducted a case study on a fish population on the Lake Bourget and compared the results to simultaneously acquired EK80 hydroacoustic data. Similar comparative methods were previously employed successfully (Rautureau et al. 2022).

On a yearly basis, the survey aims at monitoring white fish (*Coregonus lavaretus*) using a split-beam echo sounder EK80 (120 kHz, SIMRAD) (Bourinet et al. 2023). Fish size usually ranges from 10 to 50 cm. Methods and protocols for such surveys have been already explored and yielded reliable results (Mouget et al. 2019a). In this 2019 experiment, hydroacoustics data were simultaneously acquired with SeapiX (150 kHz, Exail) multi-beam echo sounder on board the Antares, a ship from the fleet of INRAE. Both echo sounders were mounted on the same side of the ship (the port side), the EK80 transducer being 0.5 m forward of the SeapiX transducer array. Both were mounted on a metal flange. Pulse length for EK80 and SeapiX was set to 256 μs. The pulse type was tone burst. The ping rate was set to 100 ms on SeapiX allowing a constant ping rate of 10 pings/s. The EK80 used the auto ping rate parameter to adjust the best rate according to the depth bottom, close to the SeapiX one. Surveys were performed in accordance with standard protocols (Drastık et al. 2017) at night between 6:20 p.m. and 0.40 a.m. in order to observe the fish population widely scattered in the water column. There was a mean speed of 2.5 knots. Hydroacoustic data from the MBES and SBES devices were processed using Echoview 11®. Prior to the survey, calibration was performed on a Tungsten carbide (WC) with a 6% cobalt binder standard sphere of 21 mm in diameter during the day. The WC sphere was suspended at 18 m in a thin monofilament line, by 60 m depth. The knots were tightened using the procedure described by Demer et al. (2015). For the EK80, calibrations were performed according to the standard protocol described by Foote et al. (1987) and the manufacturer's manual. Environmental parameters were checked during lake survey monitoring (Rimet et al. 2020) and did not change during the acoustic survey (temperature = 19.5°C, salinity = 0 psu, pH = 8). The weather was very calm during the survey and calibration procedures, with variable wind being very weak and no waves.

Signal processing using Echoview

This section details a simplified signal processing workflow utilizing Echoview, with variations between echo sounders highlighted at each step. This process is visually represented in Fig. 3.

Denoising

Denoising involves primarily removing background noise. For the EK80, we initially estimated the background noise level and then subtracted it from the data set. The algorithm employed (De Robertis and Higginbottom 2007) is widely used for echo sounder background noise removal. In the case of multi-beams, the strategy involves measuring static elements (background noise) and removing them when the target levels significantly surpass the noise level. The denoising processes are implemented in Echoview's toolbox.

Interference removal

An interference is an outlier in the output data. To remove the outliers, we applied a 3 × 3 median filter (i.e. a low-pass filter). The outliers can be partly considered as impulse noise; algorithms to process them have been put forward by Ryan et al. (2015). These methods are also implemented in Echoview's dataflow as operators.

Target detection

A target represents the amalgamation of all the detections of the same fish. Target detection consists essentially of a fish tracking algorithm. In practical terms, following denoising and interference removal steps, the image underwent binarization. The threshold for binarization was set manually, typically owning to a priori information of the TS of the target. The binarized image was then applied as a mask for the original data.

The masked output was then input into the target detection algorithm from Echoview. This preprocessing was performed on both EK80 and SeapiX datasets before applying the target detection operation.

EK80 target detection operation

Beam compensation of the EK80 was performed in Echoview with the single target detection operator. This operator aggregates single targets from the split-beam data operator that applies compensation based on split-beam angle data.

SeapiX target detection operation

The Echoview® multibeam target detection operator was used. That process was performed on both transverse and longitudinal swaths, hence the two parallel processes described in Fig. 3. Where these process lines merged in Fig. 3, the symbol ⊗ was used as the intersection operator. This operator returned all the single targets that existed in both transverse and longitudinal swaths within the acoustic transmitted beam of 1.6°. Finally, a threshold on the intensity variation was applied to finalize the detection.

For both EK80 and SeapiX, the TS threshold was set to −60 dB for SED according to monitoring surveys in the lakes (Drastik et al. 2017). This threshold allowed fish length detection >0.02 m using Love's equation (Richard and Love 1971), which is commonly used in freshwater surveys (Emmrich et al. 2012, Morrissey-McCaffrey et al. 2018, Tessier et al. 2019). The targets of interest corresponding to the white fish (*Coregonus lavaretus*) were located between 18 and 60 m depth. All the data analysed in the following sections corresponds to this layer.

Comparing results

A precise method to assess the similarity of TS distributions involves utilizing the Bhattacharyya distance: Let P_1 and P_2 be the probability density functions (estimated as histograms) of the *in situ* TS measured from the SeapiX and EK80, respectively. The Bhattacharyya distance is a statistical measure used to quantify the similarity of the two probability distributions. For discrete probability mass functions P_1 and P_2 on the same domain χ, the Bhattacharyya distance D_B is defined as follows (Bhattacharyya 1946):

$$D_B(P_1, P_2) = -\ln\left(\sum_{\chi}\sqrt{P_1(x)\,P_2(x)}\right), \qquad (10)$$

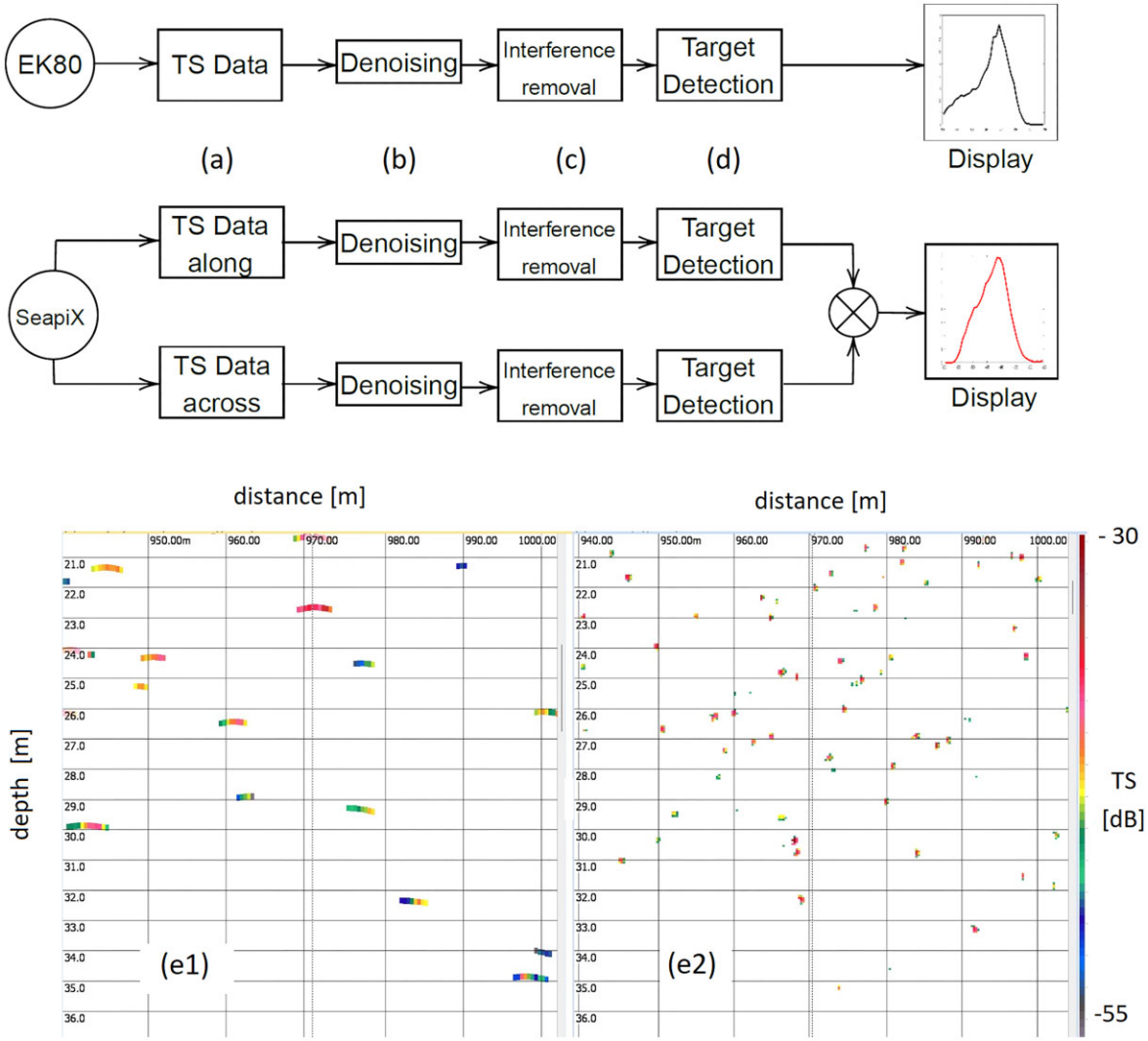

Figure 3. Simplified Echoview workflow for EK80 and SeapiX data. For both echo sounders, the workflow is similar, being: (a) extract TS, (b) denoising, (c) interference removal, and (d) target detection. For SeapiX, this process is done for transversal and longitudinal data in parallel. The intersection of both detections is then considered as the actual detection. (e1) EK80 echogram and (e2) SeapiX echogram on ± 21° simultaneously acquired.

where $P_1(x)$ and $P_2(x)$ are the probabilities of occurrence for the xth sample. The Bhattacharyya distance ranges from 0 to infinity, where 0 indicates identical distributions and infinity indicates completely dissimilar distributions.

Equation 10 can then be used to calculate the difference between the measured distributions of EK80 and SeapiX.

Results

Qualitative analysis

In this experiment, 7559 individual targets were extracted from the split-beam EK80, and 17 327 individual targets were extracted from the SeapiX data for entire swaths. The TS analysis range was from 18 to 60 m. A total of 86 727 pings were recorded with the SeapiX and 73 565 pings with the EK80. This means that the ratio of the detected single echoes to the total number of pings reaches 10.28% with the EK80 and 19.98% with SeapiX. To take advantage of measured target spatialization from the MBES data, target distribution was extracted from several directions. In this manner, 7° beam width was emulated at directions 0°, 7°,14°, and 21°. To conserve a large number of targets for distributions' plotting, port and starboard data were deliberately merged, as depicted in Fig. 4f–h. This choice was made based on the observation that detections from port and starboard are equally unbiased. This finding was visible in the quantile–quantile plot (Q–Q plot) in Fig. 5.

The Q–Q plot in Fig. 5a contains 3080 targets from the port side and 2709 from the starboard side. Figure 5b contains 2219 targets from the port side and 2311 from the starboard side, and finally, the Q–Q plot in Fig. 5c contains 1870 targets from the port side and 1915 from the starboard side. These three Q–Q plots exhibited a linear pattern around the main mode of the distribution. In one of the three plots, Fig. 5a, a diverging pattern of the 7° Q–Q plot occurs in the upper side of the curve (between −30 and −25 dB), where a few targets remained and therefore where the data were not statistically significant. Targets extracted regardless of beam direction exhibited the same modal distribution as in a traditional EK80 survey. A slight shift in the distribution toward a lower TS might come from fish statistical angular response. Considering the 0° beam only (non-steered), the TS distributions from

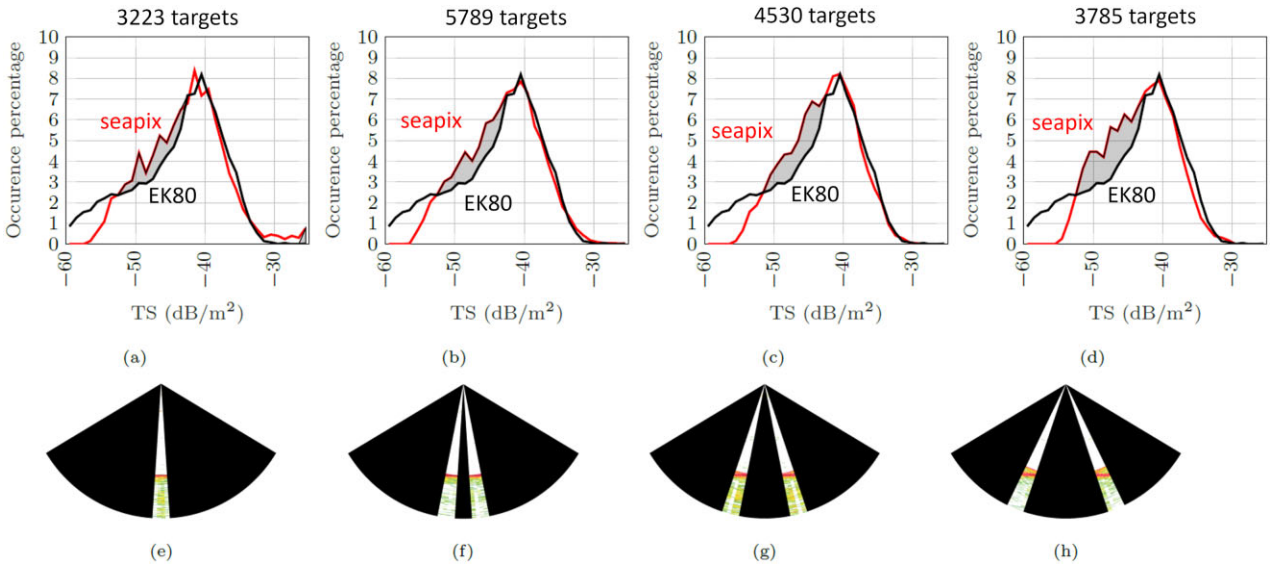

Figure 4. Superposition of the TS distribution of the 18–60 m fish layer. Various beams were considered, from left to right: (a, e) 0°, (b, f) 7°, (c, g) 14°, and (d, h) 21°. We observed that regardless of the beam angle considered, the SeapiX measurements fit with those of EK80. In gray, we have highlighted the difference between distributions as the steering angle increases.

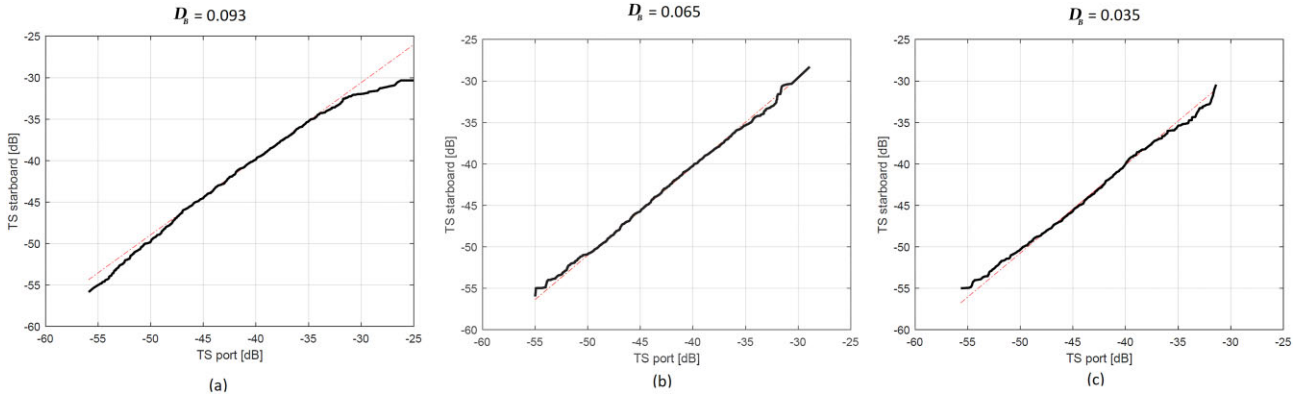

Figure 5. Q–Q plot for an emulated 7° beam width. (a) steered 7° port and starboard, which is corresponding to Fig. 4f, (b) steered 14° port and starboard, which is corresponding to Fig. 4g, and (c) steered 21° port and starboard, which is corresponding to Fig. 4h.

EK80 (120 kHz) and SeapiX (150 kHz) were superimposed, as shown in Fig. 4a. Considering the median, a difference of 0.18 dB between the two measurements (−42.57 dB for EK80 and −42.75 dB for SeapiX) was seen. Considering the mean, a difference of 0.74 dB (−43.92 dB for EK80 and −43.18 dB for SeapiX) was seen.

Analytical approach

Observing Fig. 6, we note that below −57 dB, the SeapiX histogram does not contain any entry. SeapiX was not configured to an appropriate sensitivity setting during this survey, which artificially limited the signal dynamics. We thus compare both distributions from −57 dB. By using Equation (10), we calculated that the Bhattacharyya distance between P_1 and P_2 is equal to 0.128. It means that the probability distributions behind SeapiX and EK80 measurements are hardly distinguishable. This ascertains that TS records from MBES are similar to TS records from the EK80 SBES.

Pushing further the analysis, the Bhattacharyya distance was calculated between TS distributions extracted from EK80 and SeapiX 7° emulated beam width. Table 1 provides a summary of all the Bhattacharyya distances to compare SeapiX and EK80.

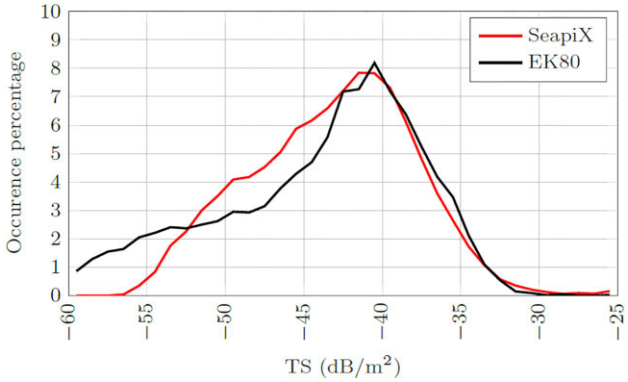

Figure 6. Overall superposition of the TS distribution of the 18–60 m fish layer.

Table 1. Bhattacharyya distance SeapiX–EK80.

	All beams (−21° to 21°)	0°	±7°	±14°	±21°
SeapiX–EK80 Bhattacharyya distance	0.128	0.134	0.129	0.132	0.132

Bhattacharyya distance calculation between SeapiX TS distribution and EK80 distribution is close to 0.130 regardless of the steering angle (0°, 7°, 14°, or 21°).

Through the application of Q–Q plots, we demonstrated an equal distribution of fish on both sides of the MBES system. To provide more insight into the Bhattacharyya distance, we also calculate associated Bhattacharyya distance on the same dataset than the one used to trace Q–Q plots. It appears these values are slightly lower than 0.1. This suggests that the level of similarity between the distributions of EK80 and SeapiX is comparable to the similarity observed within the left–right fish distributions as detected solely by SeapiX (Fig. 5a).

Discussion

A major limitation of MBES systems is their elevated side-lobe levels compared to those of SBES systems, and these can introduce ambiguities about the signal origin and diminish the signal-to-reverberation ratio. However, our study establishes that the SeapiX MBES, with its Mills cross configuration and dual-transducer array capabilities for both transmission and reception, can precisely locate targets within the beam. By excluding targets outside the primary beam, this approach effectively mitigates the issues related to high side-lobe levels in TS measurements. This pivotal functionality also enables a split-beam feature to be incorporated into the MBES. Employing signals from both arms of the Mills cross in the reception phase has also facilitated the development of innovative tools used in the acoustic characterization of dense fish shoals, demonstrating its principal merit (Tallon et al. 2020). Nevertheless, in scenarios involving fish schools or aggregations, the presence of high side lobes could potentially affect the accurate representation of fish school shapes or aggregations.

In the present study, the results illustrated in Fig. 4 show a comparison of the simulated 7° beams steered at angles of 0°, 7°, 14°, and 21°. There is a notable expansion of the area between the EK80- and SeapiX-steered distributions with an increase in the steering angle (gray area). The TS distributions measured by Seapix MBES expand toward lower TS values as the steering angle increases. The impact of fish directivity on echo sounder measurements has already been extensively studied. In a study by Cutter and Demer (2007), the Kirchoff Ray Model showed that the directivity of fish, such as walleye pollock, is close to omnidirectional in the plane perpendicular to the head-tail axis, as shown in Fig. 1b. The TS shift toward lower values could be linked to the variability of fish directivity in the "head-to-tail" direction; however, further investigations are required to validate this hypothesis.

The remaining slight differences between the two methods originate from other error sources that are common in fishery acoustic surveys and are major sources of uncertainty in echo-integration measurements. Some of these differences are due to statistical uncertainties and a slight offset in the origin of the measurement. Although pulse length and frequency affect the resolution, previous studies conducted in similar ecosystems have shown that there are no significant differences in pulse length and frequency for these kinds of targets (Godlewska et al. 2011, Guillard et al. 2014). A previous study on TS detection using the frequencies more commonly employed in freshwater (i.e. 38–200 kHz) showed no differences in scattered fish TS distribution, even if the SBES frequencies were very different (Mouget et al. 2019b). Furthermore, some differences are due to the EK80 and SeapiX beams viewing different water volumes and, hence, different fish. In the current study, the combined effect of these two features, the broad spatial coverage, and the accurate TS measurements facilitated the identification of a greater number of targets than an SBES within the same survey. This investigation concentrated on the water stratum situated between 18 and 60 m to specifically study white fish (Coregonus lavaretus), thereby inherently omitting the MBES's near field (0–11 m) and any layers below 60 m. Therefore, the long-range capabilities of SeapiX cannot be conclusively determined from this study alone. Predictive performance models suggest that SeapiX MBES can detect objects with a TS of −15 dB at a distance of 350 m under optimal conditions (sea state 0, with no additional noise from the vessel). Nevertheless, future research in deeper waters is essential to accurately evaluate the metrological performance of conducting TS assessments at such depths.

Conclusions

A quantitative analysis of TS measurements based on the distribution of fish measurements determined using MBES and SBES distributions (SeapiX MBES and EK80 split-beam, respectively) was conducted *in situ* on scattered fish in Lake Bourget, and the methods were found to produce similar results. The means and medians of the resulting distributions underscored the strong similarity between the two datasets, and the Bhattacharyya distance measurements showed that the distributions can be deemed inseparable (and thus identical). The compatibility of MBES data with information gathered through a conventional SBES demonstrates its utility for conducting a comparative analysis with historical data. The innovative solution proposed for MBES for the analysis of the major metrics of acoustic data will allow new insights into fish populations due to the inherent advantages of MBES. This compatibility allows for a seamless comparison between long-standing hydroacoustic methodologies and contemporary MBES data.

Acknowledgements

The authors wish to thank the meticulous work made by the reviewers and the editor who significantly improved the quality of this manuscript. The authors also want to thank Géraldine Duffait for her substantial work on the EVD converter and Jean-Christophe Hustache for his help in the sampling preparation and the fieldwork, as well as the Exail staff. The authors wish to thank Toby Jarvis of Echoview for his useful advice and insights and support during this project, and Patrick Schneider (Aquason) for proofreading the manuscript. We also want to mention that ISTerre is part of Labex@2020. Finally, the authors would like to extend their warmest thanks to François Gerlotto for initiating this collaboration.

Conflict of interest: The authors declare no conflicts of interest.

Funding

This work was supported by Exail SONAR and the AnaEE-France and the Observatory of LAkes (OLA) (boat and technical facilities).

Data availability

The data underlying this article will be shared on reasonable request to the corresponding author.

Author contributions

Guillaume Matte: SeapiX development, conceptualization, investigation, methodology, writing original draft. Tehei Gauthier: SeapiX development, Echoview® signal processing, Nathan Rousselot: review and editing, statistical analysis. Jean Guillard: methodology, validation, review and editing, funding acquisition, Marie Lamouret: SeapiX development, C++ software writing, validation, Olivier Lerda: SeapiX development, C++ software writing, validation, Benoit Tallon & Phillipe Roux: conceptualization, review. Frederic Mosca: SeapiX development, conceptualization, funding acquisition.

References

Bhattacharyya A. On a measure of divergence between two multinomial populations. *Sankhyā: Indian J Stat (1933-1960)* 1946;**7**:401–6. http://www.jstor.org/stable/25047882.

Bourinet F, Anneville O, Drouineau H *et al.* Synchrony in whitefish stock dynamics: disentangling the effects of local drivers and climate. *J Limnol* 2023;**82**:2134. https://doi.org/10.4081/jlimnol.2023.2134.

Colbo KTR, Brown C, Weber T. A review of oceanographic applications of water column data from multibeam echosounders. *Estuar Coast Shelf Sci* 2014;**145**:41–56. https://doi.org/10.1016/j.ecss.2014.04.002.

Cutter George R, Demer DA. Accounting for scattering directivity and fish behaviour in multibeam-echosounder surveys. *ICES J Mar Sci* 2007;**64**:1664–74. https://academic.oup.com/icesjms/article-pdf/64/9/1664/29129020/fsm151.pdf, https://doi.org/10.1093/icesjms/fsm151.

De Robertis A, Higginbottom I. A post-processing technique to estimate the signal-to-noise ratio and remove echosounder background noise. *ICES J Mar Sci* 2007;**64**:1282–91. https://doi.org/10.1093/icesjms/fsm112.

Demer DA, Berger L, Bernasconi M *et al.* Calibration of acoustic instruments. *ICES Cooperative Research Report No. 326*, International Council for the Exploration of the Sea (ICES), *Copenhagen, Denmark*, 2015. https://doi.org/10.25607/OBP-185.

Drastık V, Godlewska M, Balk H *et al.* Fish hydroacoustic survey standardization: a step forward based on comparisons of methods and systems from vertical surveys of a large deep lake. *Limnol Oceanogr Methods* 2017;**15**:836–46. https://doi.org/10.1002/lom3.10202.

Emmrich M, Winfield IJ, Guillard J *et al.* Strong correspondence between gillnet catch per unit effort and hydroacoustically derived fish biomass in stratified lakes. *Freshw Biol* 2012;**57**:2436–48. https://doi.org/10.1111/fwb.12022.

Fink G, Schmid M, Wüest A. Large lakes as sources and sinks of anthropogenic heat: capacities and limits. *Water Resour Res* 2014;**50**:7285–301. https://doi.org/10.1002/2014WR015509.

Foote KG, Knudsen HP, Vestnes G *et al.* Calibration of acoustic instruments for fish density estimation: a practical guide. *ICES Coop Res Rep (CRR)* 1987; **144**:84.

Foote KG. Optimizing two targets for calibrating a broadband multibeam sonar. In: *OCEANS 2006*. Boston, MA, USA, 2006, 1–4. https://doi.org/10.1109/OCEANS.2006.306944.

Gerlotto S, Soria M, Fréon P. From two dimensions to three: the use of multibeam sonar for a new approach in fisheries acoustics. *Can J Fish Aquat Sci*. 1999;**56**:6–12. https://doi.org/10.1139/f98-138.

Godlewska M, Colon M, Jóźwik A *et al.* How pulse lengths impact fish stock estimations during hydroacoustic measurements at 70 kHz. *Aquatic Living Res* 2011;**24**:71–8. https://doi.org/10.1051/alr/2011104.

Guillard J, Lebourges-Daussy A, Balk H *et al.* Comparing hydroacoustic fish stock estimates in the pelagic zone of temperate deep lakes using three sound frequencies (70, 120, 200 kHz). *Inland Waters* 2014;**4**:435–44. https://doi.org/10.5268/IW-4.4.733.

Love RH. Measurements of fish target strength: a review. *Fish Bull* 1971;**69**:703–15.

Mayer L, Li Y, Melvin G. 3D visualization for pelagic fisheries research and assessment. *ICES J Mar Sci* 2002;**59**:216–25. https://doi.org/10.1006/jmsc.2001.1125.

Morrissey-McCaffrey E, Rocks K, Kelly FL *et al.* Effects of differing ground-truth data, transect design and statistical analysis on the repeatability of hydroacoustic assessments of pollan *Coregonus autumnalis pollan*. *Fish Manag Ecol* 2018;**25**:304–18. https://doi.org/10.1111/fme.12295.

Mosca F, Matte G, Lerda O *et al.* Scientific potential of a new 3D multibeam echosounder in fisheries and ecosystem research. *Fish Res* 2016;**178**:130–41. https://doi.org/10.1016/j.fishres.2015.10.017.

Mouget A, Goulon C, Axenrot T *et al.* Including 38 kHz in the standardization protocol for hydroacoustic fish surveys in temperate lakes. *Remote Sens Ecol Conserv* 2019;**5**:332–45. https://doi.org/10.1002/rse2.112.

Mouget A.Including 38 kHz in the standardization protocol for hydroacoustic fish surveys in temperate lakes. In: *Remote Sensing in Ecology and Conservation*. 2019b;332–345. https://doi.org/10.1002/rse2.112.

Petitgas P, Levenez JJ. Spatial organization of pelagic fish: echogram structure, spatio-temporal condition, and biomass in Senegalese waters. *ICES J Mar Sci* 1996;**53**:147–53. https://doi.org/10.1006/jmsc.1996.0015.

Proud R, Mangeni-Sande R, Kayanda RJ *et al.* Automated classification of schools of the silver cyprinid *Rastrineobola argentea* in Lake Victoria acoustic survey data using random forests. *ICES J Mar Sci* 2020;**77**:1379–90. https://doi.org/10.1093/icesjms/fsaa052.

Rautureau C, Goulon C, Guillard J. *In situ* TS detections using two generations of echo sounder, EK60 and EK80: the continuity of fishery acoustic data in lakes. *Fish Res* 2022;**249**:106237. https://doi.org/10.1016/j.fishres.2022.106237.

Rimet F, Anneville O, Barbet D *et al.* The observatory on LAkes (OLA) database: sixty years of environmental data accessible to the public. *J Limnol* 2020;**79**:164–78. https://doi.org/10.4081/jlimnol.2020.1944.

Ryan TE, Downie RA, Kloser RJ *et al.* Reducing bias due to noise and attenuation in open-ocean echo integration data. *ICES J Mar Sci* 2015;**72**:2482–93. https://doi.org/10.1093/icesjms/fsv121.

Scalabrin C, Diner N, Weill A *et al.* Narrowband acoustic identification of monospecific fish shoals. *ICES J Mar Sci* 1996;**53**:181–8. https://doi.org/10.1006/jmsc.1996.0020.

Simmonds J, MacLennan DN. 2008. *Fisheries Acoustics: Theory and Practice*. John Wiley & Sons, Oxford UK.

Tallon B, Roux P, Matte G *et al.* Mesoscopic wave physics in fish shoals. *AIP Adv* 2020;**10**:055208. https://doi.org/10.1063/5.0005145.

Tessier A, Cottet M, Kue K *et al.* Low input of offshore areas to fisheries in a large tropical reservoir in Lao PDR. *Limnology* 2020;**21**:73–86. https://doi.org/10.1007/s10201-019-00583-1.

Handling Editor: Olav Rune Godø